A nonlocal shell model for mode transformation in single-walled carbon nanotubes

2009 J. Phys.: Condens. Matter 21 455301

(http://iopscience.iop.org/0953-8984/21/45/455301)

J. Phys.: Condens. Matter **21** (2009) 455301 (17pp) doi:10.1088/0953-8984/21/45/455301

A nonlocal shell model for mode transformation in single-walled carbon nanotubes

M X Shi[1,2], Q M Li[1,4] and Y Huang[3]

[1] School of Mechanical, Aerospace and Civil Engineering, Pariser Building, University of Manchester, PO Box 88, Manchester M60 1QD, UK
[2] Department of Engineering Mechanics, College of Science, Chang'an University, Xi'an 710064, People's Republic of China
[3] Department of Mechanical Engineering, Northwestern University, Evanston, IL 60208, USA

E-mail: Qingming.Li@manchester.ac.uk

Received 18 May 2009, in final form 8 September 2009
Published 21 October 2009
Online at stacks.iop.org/JPhysCM/21/455301

Abstract
A second-order strain gradient nonlocal shell model is established to study the mode transformation in single-walled carbon nanotubes (SWCNTs). Nonlocal length is calibrated carefully for SWCNTs in reference to molecular dynamics (MD) simulations through analysis of nonlocal length effects on the frequencies of the radial breathing mode (RBM) and circumferential flexural modes (CFMs) and its effects on mode transformation. All analyses show that only a negative second-order nonlocal shell model is appropriate to SWCNTs. Nonlocal length is evidently related to vibration modes and the radius-to-thickness ratio. It is found that a nonlocal length is approximately 0.1 nm in an average sense when RBM frequency is concerned. A nonlocal length of 0.122–0.259 nm is indicated for the mode transformation in a selected group of armchair SWCNTs. 2:1 and 1:1 internal resonances are found for the same SWCNT based on different models, which implies that the internal resonance mechanism depends on the model employed. Furthermore, it is shown that an effective thickness of approximately 0.1 nm is more appropriate to SWCNTs than 0.066 nm.

1. Introduction

Nonlocal continuum models have been successfully used to analyse the deformation and vibrations of carbon nanotubes (CNTs) (Zhang *et al* 2004, Wang and Hu 2005, Zhang *et al* 2005, Hu *et al* 2008). The key feature in nonlocal continuum theories is that the stress state at a point does not only depend on the strain state at that point, but also depends on the strain states of neighbouring points or even all the points over the whole body. This feature makes the nonlocal continuum models able to characterize deformations caused by long-range interactions between atoms in a discrete system. The increased size effects in nanoscales result in the necessity of introducing nonlocal effects in continuum models for CNTs. Since no length scale is contained in classical (local) continuum theories, they congenitally fail to predict size-dependent characteristics of microstructures. In contrast, a nonlocal length related to an internal length of microstructures (e.g. bond length or lattice parameter) can be introduced in nonlocal constitutive equations to represent size-dependent properties of the material in micro-and nanoscales. The mechanical behaviours of CNTs have been successfully predicted by nonlocal models. For example, the axial buckling strain has been investigated based on a nonlocal column model (Sudak 2003) and nonlocal shell model (Zhang *et al* 2004), which demonstrated the overestimation of the critical buckling strain by classical (local) models. In these studies, it was found that the nonlocal effects depend on the buckling mode and the length-to-radius ratio. Other studies applied nonlocal continuum models successfully to the CNT dynamics, e.g. vibrations (Zhang *et al* 2005, Duan *et al* 2007, Wang *et al* 2007) and wave propagations (Wang and Hu 2005, Hu *et al* 2008, Tounsi *et al* 2008). In the vibration of CNTs, it is found that the nonlocal effects on the natural frequency of CNTs increase with the increase of the vibration mode number.

[4] Author to whom any correspondence should be addressed.

For elastic wave propagation in CNTs, wave dispersion, which cannot be predicted by classical continuum models (Askes and Aifantis 2006), can be predicted by nonlocal continuum models (Wang and Hu 2005, Xie *et al* 2007, Hu *et al* 2008), which has been confirmed by molecular dynamics (MD) simulations (Wang and Hu 2005).

In most nonlocal analyses of CNTs, Eringen's nonlocal elasticity theory (Eringen 1983a) (often referred to as a positive second-order strain gradient nonlocal model) is directly employed because the nonlocal length in that model can be directly related to the internal length of material microstructures (Askes *et al* 2002). However, it has been shown that the second-order nonlocal model with a negative strain gradient term (referred to as a negative second-order strain gradient nonlocal model) can also contain information on material microstructure (Ioannidou *et al* 2001). A hybrid second-order nonlocal model, which includes strain inertia terms in addition to the second-order strain gradient term, was proposed (Metrikine and Askes 2002) in order to tackle the failure situations of yielding positive or finite wave propagation velocities by all the above nonlocal models (Askes and Aifantis 2006). However, the complexity of this hybrid second-order nonlocal model, especially the complexity of its energy form, prohibits its wide application (Askes and Aifantis 2006).

In all nonlocal continuum models, the nonlocal length is understood as a fixed length parameter related to the internal length of the material microstructure. Therefore, it is important to calibrate this parameter carefully first in order to yield valid predictions. A survey of nonlocal lengths (l) or equivalently the nonlocal length scale e_0 ($e_0 = l/a_{CC}$, where a_{CC} is the carbon–carbon bond length) used in nonlocal models of CNTs and the calibration procedures undertaken are summarized in table 1. In other nonlocal analyses of CNTs, Eringen's prediction of $e_0 \approx 0.39$ (Eringen 1983b) was simply adopted (Sudak 2003, Xie *et al* 2007), or a finite range of nonlocal lengths was assumed (e.g. 0–1.0 nm (Wang *et al* 2007)). Clearly, a wide range of nonlocal lengths pertaining to CNTs have been obtained from different approaches, which raises the issue of the uncertainty of this nonlocal parameter and its influence on the predicted mechanical properties and dynamical behaviours by the nonlocal model.

In the authors' recent studies on mode transformation of SWCNTs (Li and Shi 2008), classical (local) shell theory predicts that one of the two circumferential flexural modes (CFMs) 4 and 5 may be excited following the principal radial breathing mode (RBM) for an infinitely long armchair SWCNT (10, 10) (according to two effective thickness values, 0.066 nm and 0.1 nm, respectively) (Li and Shi 2008). However, it is observed in molecular dynamics (MD) simulations that CFM-3 is excited in the armchair (10, 10) (Shi *et al* 2009). This contradiction of excited CFMs is also observed for other armchair SWCNTs. Therefore, it is necessary to develop a nonlocal shell model to explain the discrepancy. For this purpose, the Goodier–McIvor thin shell model (Goodier and McIvor 1964, McIvor 1966) is extended to include nonlocal effects in the present paper. Since only RBM and CFMs with low wavenumbers are involved in vibration, the second-order strain gradient nonlocal model is adopted to establish a nonlocal Goodier–McIvor thin shell model. Frequencies of RBM and CFMs and mode transformations predicted by the proposed nonlocal model are compared with predictions from MD simulations, based on which the following two issues are carefully studied, i.e. (1) determine which one between the positive and negative second-order strain gradient nonlocal models is appropriate for the study of vibration in SWCNTs and (2) calibrate the nonlocal length.

Table 1. Summary of nonlocal lengths used for carbon nanotubes in literature and the procedures taken in calibration.

e_0	e_0a	Procedure
0–19[a]	0–2.7	Natural frequency within nonlocal Timoshenko beam theory (against MD simulations based on the COMPASS force field (Sun 1998))
		Wave propagation within nonlocal Flugge shell theory (against MD simulations based on the second-generation reactive-empirical bond order (REBO) potential (Brenner *et al* 2002))
0.2[b]	0.03	Torsional wave propagation
0.6[b]	0.08	Transverse wave propagation
0.29[c]	0.04	Wave propagation within nonlocal Timoshenko beam model (adopting the theoretical prediction of one-dimensional chain model, i.e. $d/\sqrt{12}$, d is the separation between the nearest atoms (Askes *et al* 2002))
0.82[d]	0.1	Buckling strain within nonlocal multiple shell model (against molecular mechanics simulations)
8.8[e]	1.2	Interaction between Stone–Wales and divacancy defects on carbon graphene sheet (against MD simulations)
		Wave propagation within nonlocal Timoshenko beam model
14[f]	2.0	Supporting available experimental vibration frequency ≈0.1 THz
1479[f]	210	Supporting measured vibration frequency ⩾10 THz

[a] Duan *et al* (2007). [b] Hu *et al* (2008).
[c] Wang and Hu (2005). [d] Zhang *et al* (2005).
[e] Zhang *et al* (2006a). [f] Wang (2005), Wang *et al* (2006).

2. Nonlocal Goodier–McIvor shell theory

When an infinitely long cylindrical shell undergoes deformation independent of longitudinal direction, it is reduced to a two-dimensional plane strain problem. As shown in figure 1(a), a point P on the undeformed middle surface of a thin cylindrical shell of radius a and thickness h moves to a point P* at time t. (a, θ) and (r, ϕ) are the polar coordinates of points P and P*, respectively, and the coordinates of the current position P* are functions of the coordinates of the original position P, i.e. $r = r(\theta, t)$ and $\phi = \phi(\theta, t)$. By introducing two nondimensional deformation variables ξ and ψ:

$$\xi = 1 - \frac{r}{a} \qquad \psi = \phi - \theta, \tag{1}$$

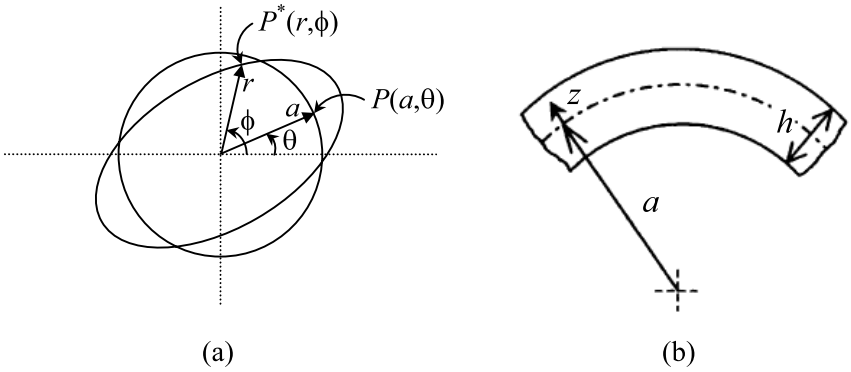

Figure 1. (a) A schematic representation of the deformation of a cylindrical shell with centroid fixed, (b) part of a shell cross section.

membrane strain ε_0 and curvature κ can be determined, respectively, as

$$\varepsilon_0 = \psi' - \xi - \xi\psi' + \tfrac{1}{2}\xi'^2, \tag{2}$$

$$a\kappa = 1 + \xi'' + \xi - (\xi'\psi')' - \xi''(\psi' - 2\xi) + \xi^2 + \tfrac{1}{2}\xi'^2, \tag{3}$$

where the prime indicates partial derivatives with respect to angle θ. In equations (2) and (3), terms higher than second order are omitted, which may affect the accuracy of numerical solutions at large time, but will not influence the flexural modes to be excited. The circumferential strain ε_θ at a point above the central line z as shown in figure 1(b) is given as

$$\varepsilon_\theta(z) = \varepsilon_0 + (1 + \varepsilon_0)(a\kappa - 1)\left(1 - \frac{z}{a}\right)\frac{z}{a}, \tag{4}$$

in which terms of order higher than $(z/a)^2$ are discarded. It may be necessary to point out that basic assumptions for small deformation of thin shells (i.e. surface normal is reserved and thickness is unchanged) are used to derive the strain expression given in equation (4). The circumferential stress σ_θ at the same point according to the second-order strain gradient nonlocal model is

$$\sigma_\theta = E_1(1 + \gamma l^2\nabla^2)\varepsilon_\theta, \tag{5}$$

where $E_1 = E/[2(1-\nu^2)]$; E is elastic modulus; ν is Poisson's ratio; l is nonlocal length; $\gamma = +1$ or -1 denoting positive or negative second-order nonlocal models. For plane strain problems, the Laplacian operator ∇^2 in equation (5) is given as

$$\nabla^2 = \frac{\partial^2}{\partial z^2} + \frac{1}{(a+z)^2}\frac{\partial^2}{\partial\theta^2} \approx \frac{\partial^2}{\partial z^2} + \left[1 - 2\frac{z}{a} + 3\left(\frac{z}{a}\right)^2\right] \times \frac{1}{a^2}\frac{\partial^2}{\partial\theta^2}. \tag{6}$$

For a circular cylindrical shell, its response can be described by the following series:

$$\xi = a_0(\tau) + \sum_{n=1}^{\infty} a_n(\tau)\cos n\theta + \sum_{n=2}^{\infty} c_n(\tau)\cos n\theta, \tag{7}$$

$$\psi = -\sum_{n=1}^{\infty} n a_n(\tau)\sin n\theta + \sum_{n=2}^{\infty} n^{-1} c_n(\tau)\sin n\theta, \tag{8}$$

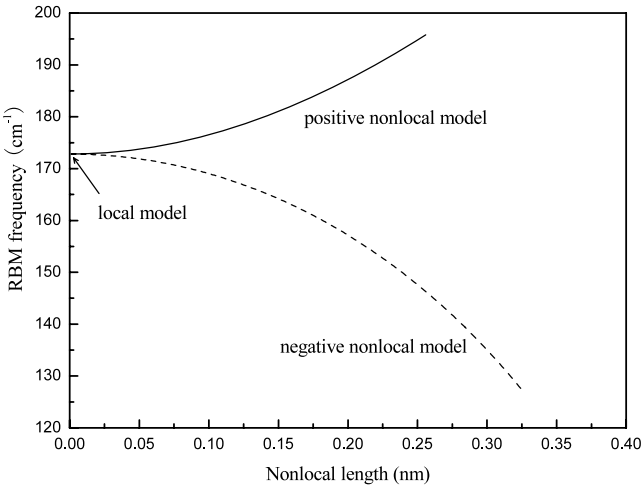

Figure 2. Nonlocal length effect on RBM frequency.

where the terms $a_n(\tau)\cos n\theta$ and $c_n(\tau)\cos n\theta$ represent extensional and inextensional flexural deformation, respectively, and $c_1(\tau)\cos\theta$ is discarded since it refers to rigid translation. The kinetic energy and potential energy of the whole system need to be defined first before the Lagrange equation is applied to derive governing equations for a_0, a_n and c_n in equations (7) and (8). For a circular cylindrical shell of unit length, the kinetic energy is given as

$$T = \frac{1}{2}\rho a h\int_0^{2\pi}\left[\left(\frac{\partial r}{\partial t}\right)^2 + \left(r\frac{\partial\psi}{\partial t}\right)^2\right]\mathrm{d}\theta = \tfrac{1}{2}E_1 a h\int_0^{2\pi}[\dot{\xi}^2 + (1-\xi)^2\dot{\psi}^2]\,\mathrm{d}\theta. \tag{9}$$

where ρ is the mass density and a dot above a symbol refers to the derivative with respect to a nondimensional time variable $\tau = tc/a$, in which phase velocity $c = \sqrt{E_1/\rho}$. The potential energy is

$$U = \int_0^{2\pi} a\,\mathrm{d}\theta\int_{-h/2}^{h/2}\tfrac{1}{2}\sigma_\theta\varepsilon_\theta\,\mathrm{d}z = \tfrac{1}{2}E_1 a\int_0^{2\pi}\mathrm{d}\theta\int_{-h/2}^{h/2}\varepsilon_\theta(1 + \gamma l^2\nabla^2)\varepsilon_\theta\,\mathrm{d}z$$

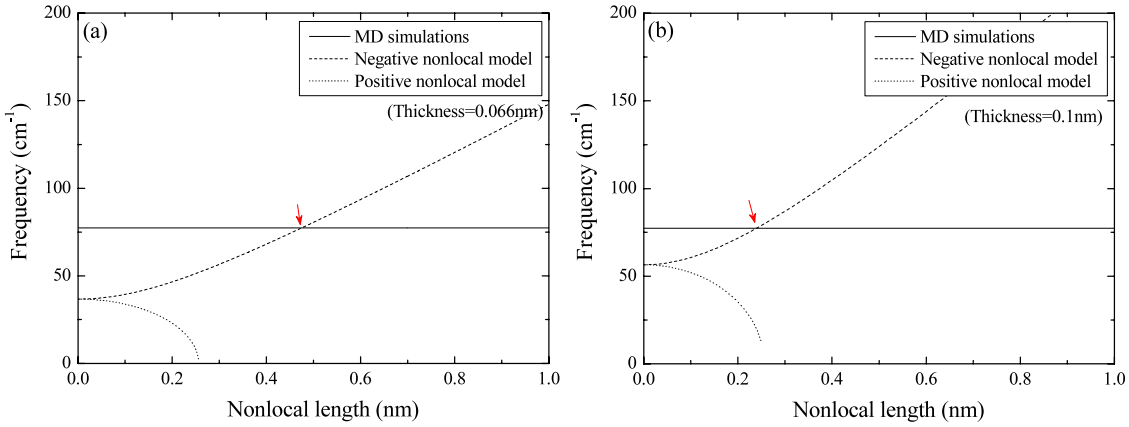

Figure 3. Variation of the frequency of inextensional flexural mode 3 versus nonlocal length in both positive and negative nonlocal models against MD simulations for armchair (10, 10): (a) thickness 0.066 nm and (b) thickness 0.1 nm.
(This figure is in colour only in the electronic version)

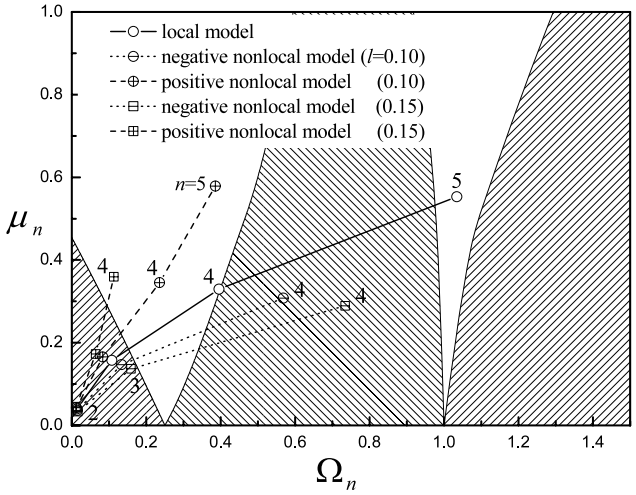

Figure 4. Mathieu stability diagram of the first two stable and unstable regions where predictions based on three models (i.e. local, positive and negative nonlocal models) are shown. In the nonlocal model, two nonlocal lengths, 0.1 and 0.15 nm, are used.

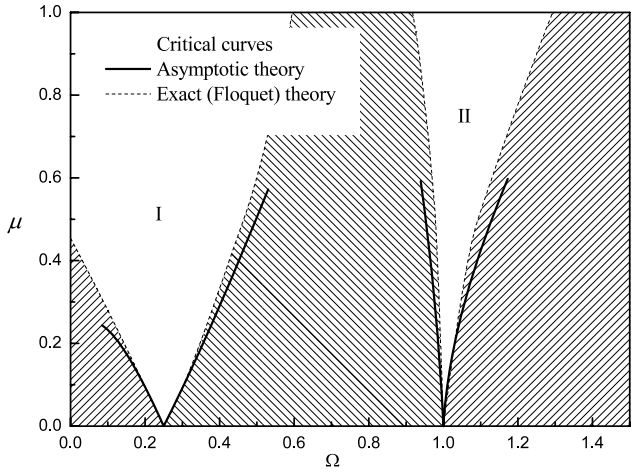

Figure 5. Critical curves in the first and second stable and unstable regions of the Mathieu stability diagram, which are determined by Floquet theory and asymptotic theory.

$$= \tfrac{1}{2}E_1 a \int_0^{2\pi} \mathrm{d}\theta \int_{-h/2}^{h/2} [\varepsilon_\theta^2 + \varepsilon_\theta \gamma l^2 \nabla^2 \varepsilon_\theta]\,\mathrm{d}z$$
$$= \pi E_1 a h [U_{\text{local}} + U_{\text{nonlocal}}], \tag{10}$$

in which the normalized potential energy part U_{local} is associated with the local elasticity theory and the other part U_{nonlocal} denotes the additional nonlocal contribution. Substituting the strain expression given by equation (4) into (10) and integrating the resulting expression along thickness leads to

$$U_{\text{local}} = \frac{1}{2\pi}\int_0^{2\pi} \mathrm{d}\theta [\varepsilon_0^2 + \alpha^2(1+\varepsilon_0)^2(a\kappa - 1)^2 - 2\alpha^2\varepsilon_0(1+\varepsilon_0)(a\kappa - 1)], \tag{11}$$

where the aspect ratio $\alpha = h/(2\sqrt{3}a)$ and

$$U_{\text{nonlocal}} = \gamma \left(\frac{l}{a}\right)^2 \frac{1}{2\pi}\int_0^{2\pi} \tilde{U}_{\text{nonlocal}}\,\mathrm{d}\theta, \tag{12}$$

where

$$\tilde{U}_{\text{nonlocal}} = -2\varepsilon_0(1+\varepsilon_0)(a\kappa - 1) + 2\alpha^2(1+\varepsilon_0)^2(a\kappa - 1)^2 + [\varepsilon_0(1+3\alpha^2) - 3\alpha^2(1+\varepsilon_0)(a\kappa - 1)]\frac{\partial^2 \varepsilon_\theta}{\partial\theta^2} + [-3\alpha^2\varepsilon_0 + \alpha^2(1+\varepsilon_0)(a\kappa - 1)] \times \frac{\partial^2}{\partial\theta^2}[(1+\varepsilon_0)(a\kappa - 1)]. \tag{13}$$

Substituting membrane strain ε_0 given by equation (2) and curvature κ given by equation (3) into equations (11) and (13), respectively, and simplifying the results leads to

$$U_{\text{local}} = \frac{1}{2\pi}\int_0^{2\pi} \mathrm{d}\theta [(\psi' - \xi)^2 + (\psi' - \xi)(\xi'^2 - 2\xi\psi') + \alpha^2(\xi + \xi'')(3\xi + \xi'' - 2\psi')], \tag{14}$$

and

$$\tilde{U}_{\text{nonlocal}} = -(\psi' - \xi)(2\xi + 3\xi'' - \psi''') - 2(\psi' - \xi)(\psi'\xi - \psi'\xi'' - \psi''\xi' + \xi\xi'' + \tfrac{1}{2}\xi'^2)$$

$$+(\psi'-\xi)(-\psi'''\xi-2\psi''\xi'-\psi'\xi''+\xi'\xi'''+\xi''^2)$$
$$+(\psi'''-2\xi-3\xi'')(-\psi'\xi+\tfrac{1}{2}\xi'^2)$$
$$+2\alpha^2(\xi+\xi'')^2+3\alpha^2(\psi'-\xi)(\psi'''-2\xi''-\xi^{(4)})$$
$$+\alpha^2(\xi+\xi'')(4\xi''+\xi^{(4)}-3\psi'''), \tag{15}$$

where $\xi^{(4)}$ indicates the fourth-order partial derivative with respect to angle θ. In equation (15), the first term $-(\psi'-\xi)(2\xi+3\xi''-\psi''')$ is of second order and is the dominant term in the nonlocal potential energy part. Now the kinetic energy and potential energy are expressed through the two nondimensional variables ξ and ψ. Substitute modal expansions of ξ and ψ given by equations (7) and (8) into the final expressions of T and U given by equations (9), (10), (14) and (15) and use generalized coordinate q_i to represent $a_0, \ldots, a_n, c_1, \ldots, c_n$ in sequence in the Lagrange equation

$$\frac{\partial}{\partial\tau}\left(\frac{\partial T}{\partial\dot{q}_i}\right)-\frac{\partial T}{\partial q_i}+\frac{\partial U}{\partial q_i}=0, \qquad i=1,2,\ldots, \tag{16}$$

we then obtain the following governing equations of a_0, a_n and c_n:

$$\ddot{a}_0+a_0(1+3\alpha^2)-\tfrac{1}{4}\sum_n^{\infty}(n^2-2)c_n^2+\tfrac{1}{2}\Pi_{a_0}=0, \tag{17}$$

$$\ddot{a}_n+(n^2+1)a_n-2\alpha^2\frac{n^2-1}{n^2+1}c_n-\frac{n^2-2}{n^2+1}a_0c_n$$
$$+\tfrac{1}{4}\sum_{m=1}^{\infty}\{[2-m(m+n)]c_mc_{m+n}$$
$$+[2-m(m-n)]c_mc_{|m-n|}\}+\frac{1}{n^2+1}\Pi_{a_n}=0, \tag{18}$$

$$\ddot{c}_n+\alpha^2\frac{n^2(n^2-1)^2}{n^2+1}c_n-\frac{n^2(n^2-2)}{n^2+1}a_0c_n+\frac{n^2}{2(n^2+1)}$$
$$\times\sum_{m=1}^{\infty}\{[2-n(m+n)]c_{m+n}+[2+n(m-n)]c_{|m-n|}\}$$
$$\times(m^2+1)a_m\frac{n^2}{n^2+1}\Pi_{c_n}=0. \tag{19}$$

In equations (17)–(19), Π_{a_0}, Π_{a_n} and Π_{c_n}, respectively, represent the contributions from the nonlocal potential energy part to the final governing equations of a_0, a_n and c_n, and are given by

$$\Pi_{a_0}=\gamma\left(\frac{l}{a}\right)^2[4a_0+\cdots], \tag{20}$$

$$\Pi_{a_n}=\gamma\left(\frac{l}{a}\right)^2[-n^2(n^2+1)^2a_n+\cdots], \tag{21}$$

$$\Pi_{c_n}=\gamma\left(\frac{l}{a}\right)^2[-\alpha^2(n^2-2)(n^2-1)^2c_n-(4n^2-6)a_0c_n+\cdots], \tag{22}$$

in which only the most dominant terms are shown. It should be noted that equations (17)–(19) have been simplified based on the fact that the amplitude of extensional flexural mode terms a_n is smaller than that of the inextensional flexural mode term c_n (Goodier and McIvor 1964). Those higher-order terms not shown in equations (20)–(22) will be included in the numerical calculations when numerical solutions are obtained. It can be easily seen from equations (17)–(22) that, given a fixed nonlocal length l, the larger the circular cylindrical shell, the smaller the nonlocal length effect on mode transformations.

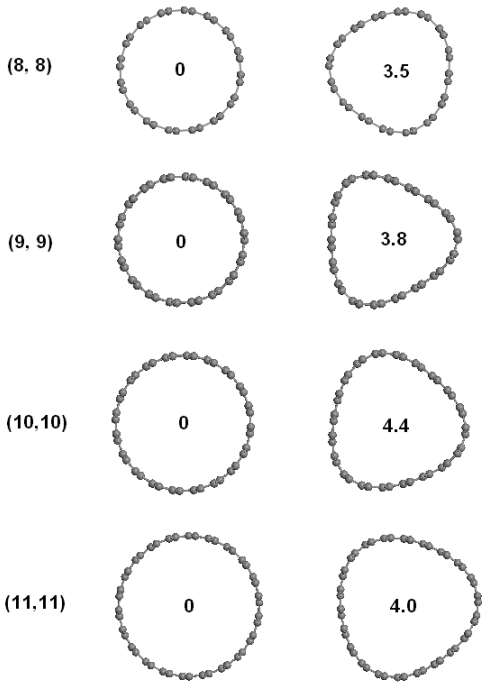

Figure 6. Cross-sectional shapes of armchairs from (8, 8) to (11, 11) at initial state and the time when the third mode of CFM (CFM-3) is first excited. The CFM initiation time has units of ps.

Now the governing equations for the in-plane vibration of a nonlocal Goodier–McIvor shell have been established, based on which numerical simulations can be performed when initial conditions are prescribed. As discussed in section 1, available values of nonlocal length in the literature vary over a wide range. Each approach used in calibrating nonlocal length focuses on one specific mechanical behaviour of CNTs and the value of nonlocal length is obtained by comparing nonlocal continuum model predictions against experimental observations or MD simulations. In the following two sections the effects of nonlocal length on the frequencies of RBM and CFMs, and on the mode transformation in SWCNTs, will be investigated, based on which it will be determined whether positive or negative nonlocal models are appropriate to CNTs and the nonlocal lengths suitable for the study of vibration and mode transformation in CNTs.

3. Nonlocal effect on frequencies of RBM and CFMS

Governing equations (17)–(19) contain nonlinear terms. When they are linearized, the governing equations of a_0, a_n and c_n are

$$\ddot{a}_0+k_{\mathrm{RBM}}^2a_0=0, \tag{23}$$

$$\ddot{a}_n+k_{\mathrm{Extensional}}^2a_n=0, \tag{24}$$

$$\ddot{c}_n+k_{\mathrm{Inextensional}}^2c_n=0, \tag{25}$$

where k_{RBM}, $k_{\mathrm{Extensional}}$ and $k_{\mathrm{Inextensional}}$ are, respectively, circular frequencies of RBM, nth extensional flexural mode

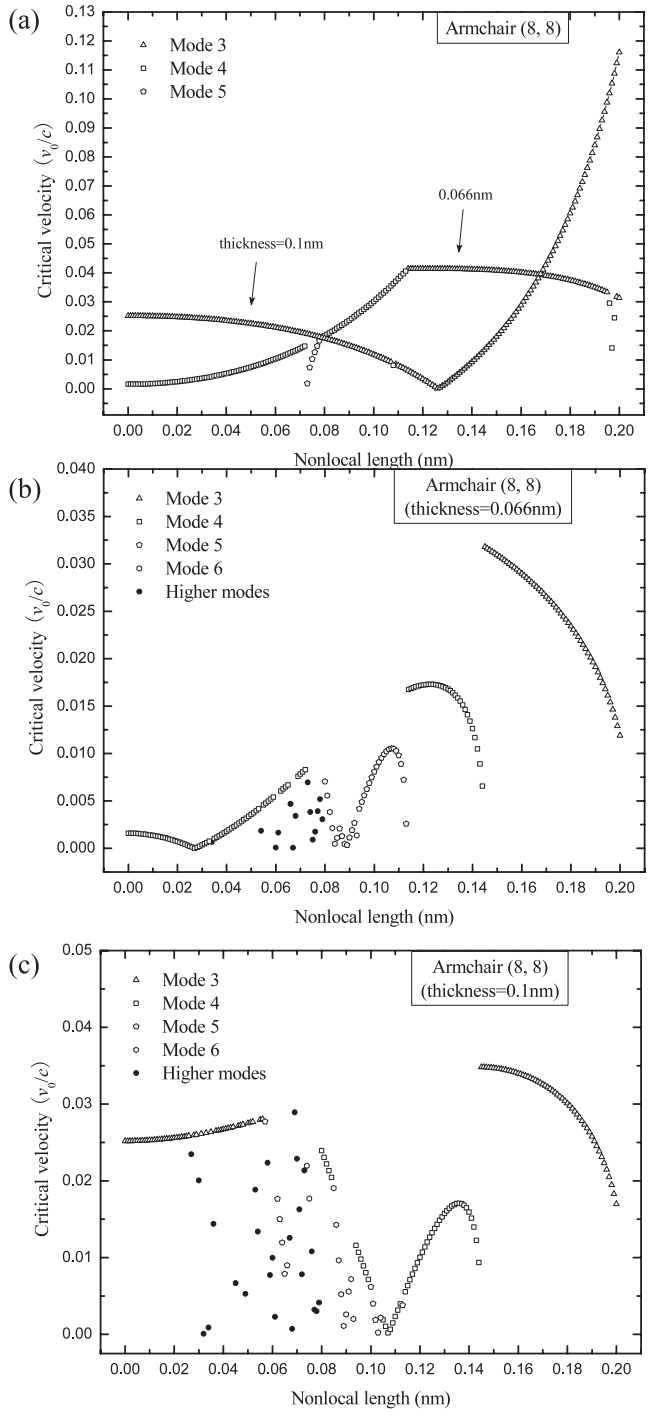

Figure 7. The most likely excited flexural mode and the critical initial velocity of armchair (8, 8) based on (a) negative nonlocal model, (b) and (c) positive nonlocal model.

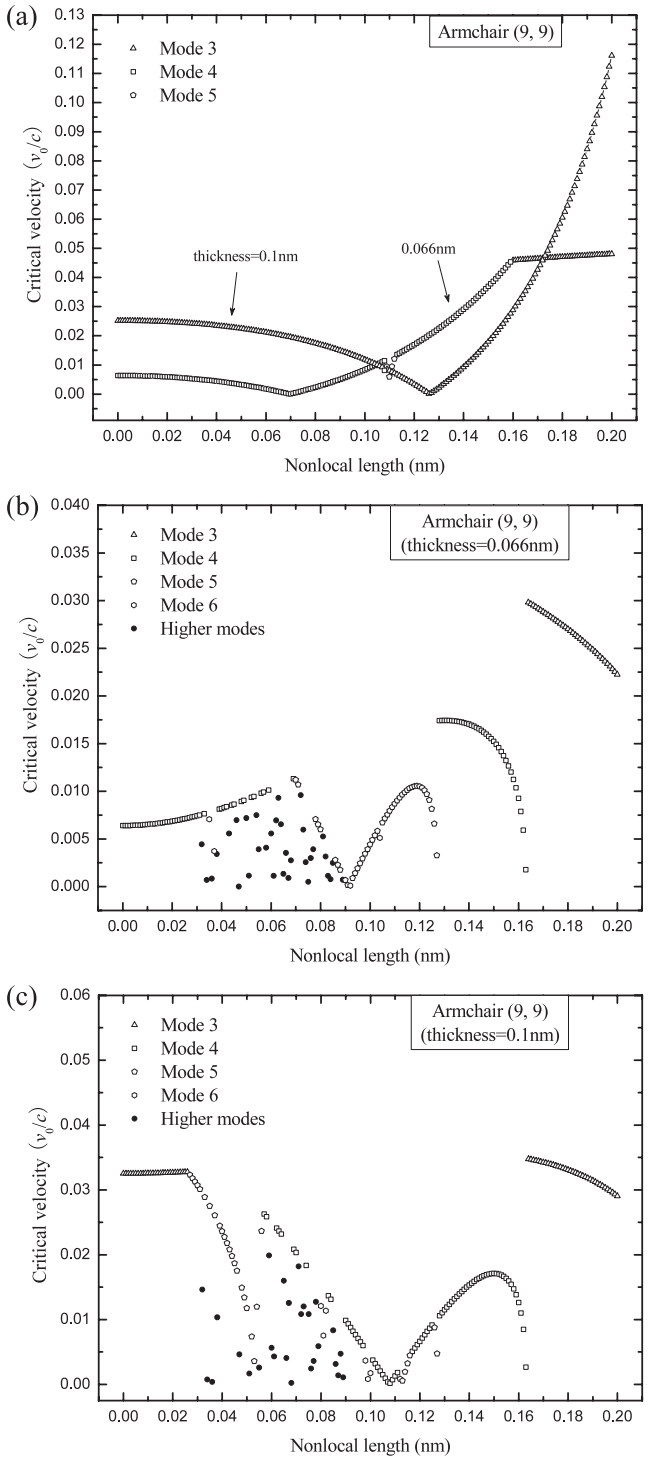

Figure 8. The most likely excited flexural mode and the critical initial velocity of armchair (9, 9) based on (a) negative nonlocal model, (b) and (c) positive nonlocal model.

and nth inextensional flexural mode, i.e.

$$k_{\mathrm{RBM}} = \sqrt{1 + 3\alpha^2 + 2\gamma\left(\frac{l}{a}\right)^2}, \tag{26}$$

$$k_{\mathrm{Extensional}} = \sqrt{(n^2+1)\left[1 - n^2\gamma\left(\frac{l}{a}\right)^2\right]}, \tag{27}$$

$$k_{\mathrm{Inextensional}} = \alpha\sqrt{\frac{n^2\left(n^2-1\right)^2}{n^2+1}\left[1 - (n^2-2)\gamma\left(\frac{l}{a}\right)^2\right]}. \tag{28}$$

Since the nondimensional time variable in equations (17)–(19) is defined as $\tau = tc/a$, then the frequency of each mode in

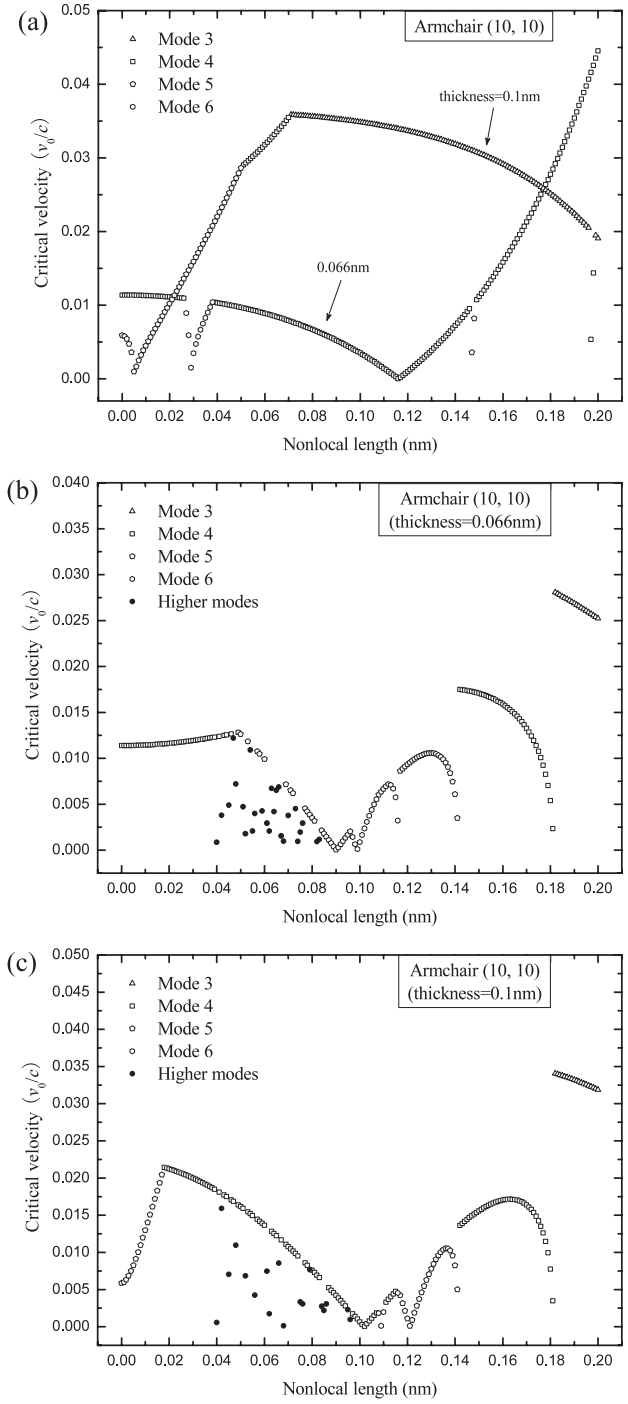

Figure 9. The most likely excited flexural mode and the critical initial velocity of armchair (10, 10) based on (a) negative nonlocal model, (b) and (c) positive nonlocal model.

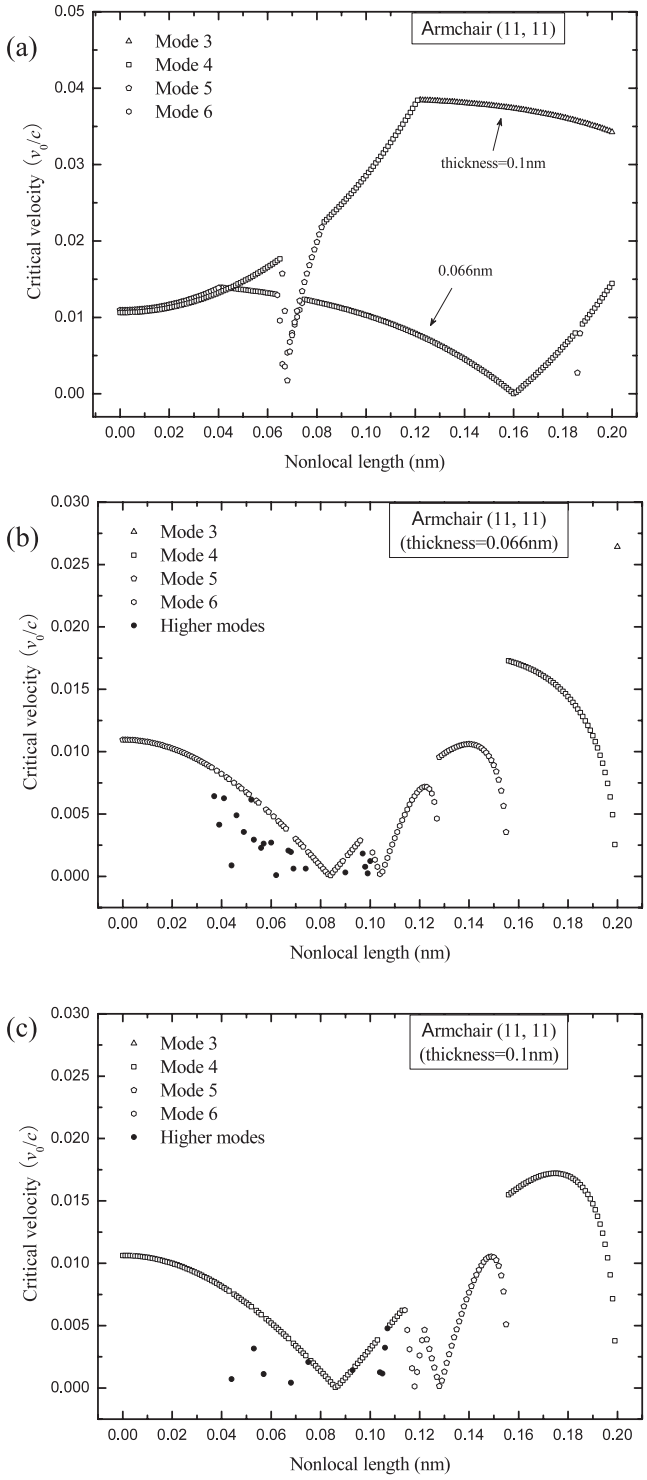

Figure 10. The most likely excited flexural mode and the critical initial velocity of armchair (11, 11) based on (a) negative nonlocal model, (b) and (c) positive nonlocal model.

units cm^{-1} can be obtained as

$$f_{\mathrm{RBM}} = \frac{1}{2\pi}\frac{c}{c_{\mathrm{light}}}\frac{1}{a}\sqrt{1+3\alpha^2+2\gamma\left(\frac{l}{a}\right)^2}\,(\mathrm{cm}^{-1}), \tag{29}$$

$$f_{\mathrm{Extensional}} = \frac{1}{2\pi}\frac{c}{c_{\mathrm{light}}}\frac{1}{a} \times \sqrt{(n^2+1)\left[1-n^2\gamma\left(\frac{l}{a}\right)^2\right]}\,(\mathrm{cm}^{-1}), \tag{30}$$

$$f_{\mathrm{Inextensional}} = \alpha\frac{1}{2\pi}\frac{c}{c_{\mathrm{light}}}\frac{1}{a} \times \sqrt{\frac{n^2(n^2-1)^2}{n^2+1}\left[1-\left(n^2-2\right)\gamma\left(\frac{l}{a}\right)^2\right]}\,(\mathrm{cm}^{-1}). \tag{31}$$

In equations (29)–(31) $c_{\text{light}} = 2.998 \times 10^{10}$ cm s^{-1} is the speed of light. From the formula for f_{RBM}, $f_{\text{Extensional}}$ and $f_{\text{Inextensional}}$ given by equations (29)–(31), in order to avoid an imaginary frequency value for each of them, it can be easily seen that there exist nonlocal length upper limits for f_{RBM} within the negative nonlocal model and for $f_{\text{Extensional}}$ and $f_{\text{Inextensional}}$ within the positive nonlocal model. Comparing f_{RBM} with $f_{\text{Extensional}}$, it can be found that in the local shell model, when the small term $3\alpha^2$ (compared to 1) in f_{RBM} is neglected, f_{RBM} is equivalent to the case of $f_{\text{Extensional}}$ with $n = 0$. Assume that the nonlocal length l is of the order of thickness h of SWCNTs, and $(l/a)^2$ and α^2 in the expression of f_{RBM} are smaller terms in comparison to unity, then

$$\begin{aligned} f_{\text{RBM}} &= \frac{1}{2\pi}\frac{c}{c_{\text{light}}}\frac{1}{a}\sqrt{1+3\alpha^2\left[1+8\gamma\left(\frac{l}{h}\right)^2\right]} \\ &\approx \frac{1}{2\pi}\frac{c}{c_{\text{light}}}\frac{1}{a}\left\{1+\frac{3}{2}\alpha^2\left[1+8\gamma\left(\frac{l}{h}\right)^2\right]\right\} \\ &= \frac{A}{a}+\frac{B}{a^3}, (\text{cm}^{-1}) \end{aligned} \tag{32}$$

in which

$$A = \frac{1}{2\pi}\frac{c}{c_{\text{light}}}, \tag{33a}$$

$$B = \frac{1}{16\pi}\frac{c}{c_{\text{light}}}\left[1+8\gamma\left(\frac{l}{h}\right)^2\right]h^2. \tag{33b}$$

Therefore

$$f_{\text{RBM}} = \frac{A}{a}\left[1+\left(\frac{h}{a}\right)^2\left(0.125+\gamma\left(\frac{l}{h}\right)^2\right)\right]. \tag{34}$$

RBM is one of the most important modes of SWCNTs. RBM frequency with varying nonlocal lengths within both positive and negative nonlocal models are plotted in figure 2 through an example of armchair (10, 10). It can be seen that the nonlocal length in positive and negative second-order nonlocal models influences the RBM frequency in opposite ways.

The expression of RBM frequency f_{RBM} given in equation (34) shows that the term A/a is dominant. In order to determine the dominant term A/a, the phase velocity c of CNTs defined as $\sqrt{\frac{E}{\rho(1-\nu^2)}} = \sqrt{\frac{Eh}{\rho h(1-\nu^2)}}$ is estimated. The reported in-plane stiffness Eh is between 300 and 422 J m^{-2} (Wang and Zhang 2008). The mean value $Eh = 360$ J m^{-2} supports experiments and theoretical evaluations reasonably well (Wang and Zhang 2008), which will be used in this study. The transverse mass density is $\rho h = 7.72 \times 10^{-7}$ kg m^{-2} and Poisson's ratio $\nu = 0.19$ according to MD simulations (Yakobson *et al* 1996). Thus, the phase velocity of SWCNTs is estimated to be $c \approx 22.0$ km s^{-1}.

The thickness concept of an SWCNT is only associated with macroscopic continuum models as a real SWCNT is a collection of discrete carbon atoms. A range of SWCNT effective thicknesses from 0.0617 to 0.69 nm has been indicated based on different approaches (Wang and Zhang 2008). Next, we will determine its value based on two important concepts, i.e. in-plane stiffness Eh and in-plane bending stiffness $D = Eh^3/[12(1-\nu^2)]$. The in-plane stiffness Eh is given as 360 J m^{-2}, as just discussed above. The in-plane bending stiffness $D = 0.85$ eV was suggested in Yakobson *et al* (1996), which leads to an effective thickness of 0.066 nm. Recent *ab initio* calculations predicted the in-plane bending stiffness D in a range of 1.95–2.16 eV with a mean value 2.0 eV (Wang *et al* 2005). Thus, when $D = 2.0$ eV, $Eh = 360$ J m^{-2} and $\nu = 0.19$, another effective thickness of SWCNTs can be determined approximately as 0.1 nm. In the following analysis, two values of the effective thickness of SWCNTs, i.e. 0.066 nm and 0.1 nm, will be used respectively for parametric sensitivity analysis.

Given $c \approx 22.0$ km s^{-1} and $c_{\text{light}} = 2.998 \times 10^{10}$ cm s^{-1}, the factor A in the approximate expression of f_{RBM} given by equation (33) can be determined as 116.7 nm cm^{-1}, which agrees very well with the fitted constant of $A = 117$ nm cm^{-1} in Kurti (1998) and $A = 116.6$ nm cm^{-1} in Sanchez-Portal *et al* (1999). Thus, for armchair (10, 10) (radius $a = 0.678$ nm), $A/a = 172.8$ cm^{-1}. Then, according to equation (34), if the actual RBM frequency of armchair (10, 10) is smaller than 172.8 cm^{-1}, the sign factor γ in the nonlocal model must be negative, which implies that the negative second-order nonlocal model should be adopted for RBM of SWCNTs. Otherwise, the positive second-order nonlocal model should be adopted. RBM frequency values of armchair (10, 10) have been reported in the literature, e.g. 165.0 cm^{-1} (Rao *et al* 1997, Kuzmany *et al* 1998), 169.0 cm^{-1} (Lawler *et al* 2005) and 174–175 cm^{-1} (Kurti 1998). Since the reported RBM frequency values of armchair (10, 10) are either below or above 172.8 cm^{-1}, it is difficult to use these data to determine whether a positive or negative second-order nonlocal model is appropriate for the modelling of SWCNTs.

In line with the present mode transformation analysis of SWCNTs, MD simulations are carried out here for frequency analysis of SWCNTs using commercial software *Material Studio* (Accelrys 2008). Atomic force field *COMPASS* (condensed phase optimized molecular potentials for atomistic simulation studies) is employed to govern motions of all atoms through the *Discover* module of the software. The parameters of the *COMPASS* force field are derived from *ab initio* quantum mechanics calculations (Sun 1998, Sun *et al* 1998). A selection of armchairs from (8, 8) to (11, 11) are chosen for MD simulations since their geometry aspect ratios α are among the range approximately suitable for the nonlocal shell models and experimental identifications of them are reported (Rao *et al* 1997). The MD simulation results of RBM frequency for all the armchairs are presented in table 2, in which the calculated values of A/a are also included. It shows that the calculated values of A/a for all the selected armchairs are consistently larger than the corresponding MD predictions, and therefore a negative second-order strain gradient nonlocal term is required to compensate for the difference between A/a and MD prediction for each armchair. Values of the nonlocal length for all selected armchairs can be calculated by matching RBM frequencies based on equation (34) with the corresponding MD predictions and the results are also listed in table 2. In order to check the sensitivity of calculated nonlocal length to

Table 2. RBM frequency of armchairs from (8, 8) to (11, 11) from MD simulations and the calculated nonlocal length in the negative nonlocal model for each armchair based on equation (34). Two cases are studied: thickness $h = 0.066$ nm and 0.1 nm, respectively.

				l (nm)	
Armchair	a (nm)	f_{RBM} (cm^{-1})	A/a	$h = 0.066$ nm	$h = 0.1$ nm
(8, 8)	0.542	211.87	215.31	0.073	0.078
(9, 9)	0.610	187.54	191.31	0.090	0.094
(10, 10)	0.678	168.01	172.12	0.109	0.112
(11, 11)	0.746	152.10	156.43	0.128	0.131

thickness, two thickness values, 0.066 nm and 0.1 nm, are used respectively in the determination of nonlocal length. It is found that the calculated nonlocal lengths for the same armchair are very close to each other for these two different thickness values, and therefore nonlocal length is not sensitive to the thickness regarding RBM frequency. This is important since hitherto no unique effective thickness value of SWCNTs has been accepted in the literature. However, nonlocal length is clearly dependent on the armchair radius or on the radius-to-thickness ratio for a given wall thickness in respect of RBM frequency. Since the present nonlocal model can only deal with fixed nonlocal length and RBM is the initial vibration mode that may excite CFMs due to an internal resonance mechanism, we use the average of calculated nonlocal length values as a representative nonlocal length in further analyses. Based on the data in table 2, the average nonlocal length l is determined as 0.100 nm (for $h = 0.066$ nm) and a close value of 0.104 nm (for $h = 0.1$ nm), which accordingly gives B in equation (33) as -1.10 and -1.02 cm^{-1} nm^3, respectively. Therefore a representative nonlocal length for SWCNTs is taken as $l \approx 0.1$ nm, or nonlocal length scale $e_0 = l/a_{\mathrm{CC}} \approx 0.7$. The term containing nonlocal length dominates the expression of B, and therefore, in the RBM expression given by equation (32), B/a^3 represents a nonlocal correction of the dominant RBM frequency term A/a.

However, it might be argued that the approach using the expression $f_{\mathrm{RBM}} = A/a + B/a^3$ to evaluate the nonlocal length may be questionable since B/a^3 is much smaller than the dominant term A/a. (Note: according to equations (33*a*) and (33*b*), $|\frac{B/a^3}{A/a}| = \frac{3}{2}|1 + 8\gamma(\frac{l}{h})^2|\alpha^2$, which, considering the assumption that the nonlocal length is of the order of the thickness, will be of the order of α^2, and therefore this ratio is much smaller than unity because the squared aspect ratio $\alpha^2 = h^2/(12a^2)$ is a higher-order small term.) Therefore, more careful examination of nonlocal length is necessary. Next, frequencies of low CFMs will be compared between nonlocal model predictions and MD simulations, based on which it will be determined again whether the positive or negative nonlocal model should be adopted for SWCNTs and meanwhile nonlocal length will be calibrated. First, frequencies of CFMs from MD simulations are obtained for the selected armchairs and the results including RBM frequency are given in table 3. It can be seen from the table that frequencies of CFM-2 to CFM-4 for each armchair are smaller than the RBM frequency, and therefore they should belong to inextensional flexural modes since RBM in the local shell

Table 3. RBM and CFM frequencies (from mode 2 to mode 7) based on *ab initio* MD simulations.

		CFM					
Armchair	RBM	2	3	4	5	6	7
(8, 8)	211.87	42.99	112.85	207.99	316.06	429.90	529.50
(9, 9)	187.54	34.42	92.78	172.61	265.01	367.82	470.03
(10, 10)	168.01	26.96	77.42	144.85	224.32	314.66	409.39
(11, 11)	152.10	20.71	65.46	123.07	191.55	270.76	355.99

Table 4. Nonlocal lengths for various CFMs for a range of armchair SWCNTs.

	$h = 0.066$ nm			$h = 0.1$ nm		
Armchair	2	3	4	2	3	4
(8, 8)	0.716	0.347	0.232	0.363	0.163	0.103
(9, 9)	0.820	0.411	0.280	0.420	0.202	0.133
(10, 10)	0.872	0.475	0.325	0.434	0.240	0.161
(11, 11)	0.870	0.538	0.372	0.399	0.277	0.188
Average	0.820	0.443	0.302	0.404	0.221	0.146

model is equivalent to the extensional flexural mode with $n = 0$ and the nonlocal contribution to CFM frequency is secondary in comparison with the local contribution. Take armchair (10, 10) as an example: variation of the frequency of inextensional flexural mode 3 versus nonlocal length within positive and negative nonlocal models are plotted against MD simulations, respectively, in figure 3(a) for a thickness of 0.066 nm and (b) for a thickness of 0.1 nm. Due to the similarity, frequencies of inextensional flexural modes 4 and 5 within the two nonlocal models are not plotted.

The graphs in the above figure show that the positive nonlocal model is incapable of predicting the same frequency of inextensional flexural mode 3 predicted by MD simulations. Therefore, only the negative nonlocal model is appropriate to nonlocal modelling of SWCNTs. The fitted nonlocal length values within the negative nonlocal model for low CFMs (2, 3 and 4) against MD simulations are listed in table 4. Clearly, the fitted nonlocal length is related to both the effective thickness of SWCNTs and the wavelength of CFMs, which supports available reports in the literature (Zhang *et al* 2005, Duan *et al* 2007, Hu *et al* 2008).

4. Nonlocal effect on mode transformation

When a circular cylindrical shell is subjected to a nearly uniform radial impulse, without losing generalities, the initial conditions of nondimensional variables ξ and ψ can be described by

$$\xi(\theta, 0) = \psi(\theta, 0) = 0, \tag{35}$$

$$\dot{\xi}(\theta, 0) = \frac{1}{c}\left(v_0 + \sum_{n=1}^{\infty} v_n \cos n\theta\right), \qquad \dot{\psi}(\theta, 0) = -\frac{v_1}{c}\sin\theta. \tag{36}$$

In the above equations, v_0 stands for a perfectly uniform radial velocity and v_n terms represent the imperfections, which are normally at least two orders smaller than v_0. Equations (35)

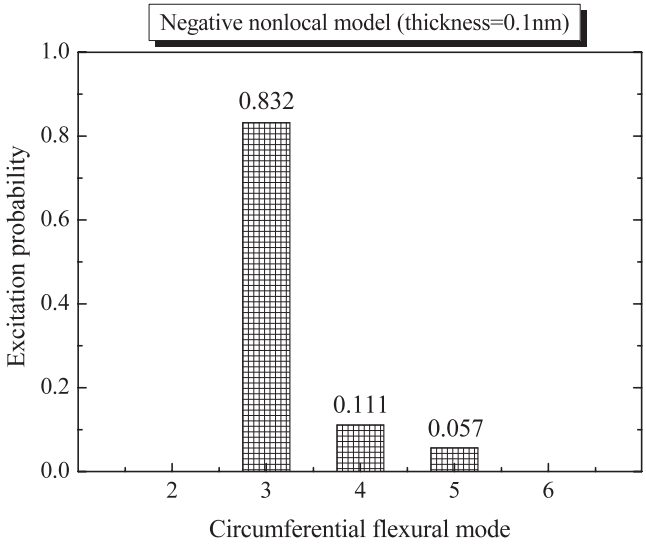

Figure 11. Excitation probability of CFMs based on negative nonlocal model as nonlocal length varies in a range 0–0.5 nm for armchairs from (8, 8) to (11, 11) with thickness 0.1 nm.

and (36) together with equations (7) and (8) give the initial conditions for a_0, a_n and c_n in the governing equations (17)–(19), i.e.

$$a_0(0) = 0, \qquad \dot{a}_0(0) = \frac{v_0}{c}, \tag{37a}$$

$$a_1(0) = 0, \qquad \dot{a}_1(0) = \frac{v_1}{c}, \tag{37b}$$

$$a_n(0) = 0, \qquad \dot{a}_n(0) = \frac{1}{n^2+1}\frac{v_n}{c}, \qquad n \geqslant 2 \tag{37c}$$

$$c_n(0) = 0, \qquad \dot{c}_n(0) = \frac{n^2}{n^2+1}\frac{v_n}{c}, \qquad n \geqslant 2. \tag{37d}$$

Initially, the amplitudes of c_n ($n \geqslant 2$) are small because the imperfections are small in initial condition equations (37*a*)–(37*d*). When the terms c_n are omitted in equation (17), it is reduced to the linear equation (23). A harmonic vibration solution of equation (23) with initial condition given in equation (37*a*) can be easily obtained as

$$a_0 = \frac{v_0}{k_{\mathrm{RBM}}c}\sin(k_{\mathrm{RBM}}\tau) = \frac{v_0}{k_{\mathrm{RBM}}c}\sin\left(k_{\mathrm{RBM}}\frac{c}{a}t\right). \tag{38}$$

With the solution of a_0 and the assumption of $|a_m| \ll |c_m|$, ($m \geqslant 2$) (since it is reasonably assumed that, for thin shells, the coupling between RBM and the inextensional flexural modes is much stronger than that between RBM and the extensional flexural modes (Goodier and McIvor 1964)), the governing equation (19) of c_n can be reduced to a Mathieu-type equation:

$$\ddot{c}_n + (\Omega_n - \mu_n \sin\eta)c_n = 0, \tag{39}$$

where

$$\Omega_n = \frac{n^2(n^2-1)^2}{n^2+1}\left[1 - (n^2-2)\cdot\gamma\left(\frac{l}{a}\right)^2\right]\frac{1}{k_{\mathrm{RBM}}^2}\alpha^2, \tag{40}$$

$$\mu_n = \frac{n^2}{n^2+1}\left[n^2 - 2 + (4n^2-6)\cdot\gamma\left(\frac{l}{a}\right)^2\right]\frac{1}{k_{\mathrm{RBM}}^2}\frac{v_0}{c}, \tag{41}$$

in which the new nondimensional time variable η is given as $\eta = k_{\mathrm{RBM}}\tau$. When γ is set as zero, the governing equation of c_n, equation (40), will revert to the equation in classical (local) elasticity shell theory (i.e. equation (48) in Goodier and McIvor 1964).

The procedure for the determination of mode transformation is described below. For a circular cylindrical shell with given initial conditions, the pair of parameters (α, v_0/c) are calculated. Then, points (Ω_n, μ_n) are calculated for various flexural vibration mode numbers n. If one or more points of (Ω_n, μ_n) fall in any unstable region of the Mathieu stability diagram (unshaded areas in figure 4), the corresponding flexural vibration mode(s) n can be excited from the initial RBM, which represents the occurrence of mode transformation between RBM and CFM(s). The nonlocal contributions to the values of (Ω_n, μ_n) are related to $\gamma(l/a)^2$, as shown in equations (40) and (41). The nonlocal length effect on mode transformation will be analysed in two steps.

In the first step, the nonlocal length effect on mode transformation is investigated in a qualitative sense and a circular cylindrical shell of armchair (10, 10) is taken as an example. Using the radius $a = 0.678$ nm and thickness $h = 0.1$ nm, its aspect ratio is $\alpha = h/(\sqrt{12}a) = 0.043$. Given initial velocity $v_0/c = 0.025$ and two nonlocal lengths of 0.1 nm and 0.15 nm, respectively, all the points (Ω_n, μ_n) in the first two stable and unstable regions of the Mathieu stability diagram are shown in figure 4, which leads to the following observations.

(1) Nonlocal length effect on the values of (Ω_n, μ_n), and thus on mode transformation, is stronger for higher modes of CFMs (e.g. modes 4 and 5) than for lower modes (e.g. modes 2 and 3). Such an influence increases remarkably as mode number increases. This observation agrees qualitatively with other investigations on nonlocal effects (Sudak 2003, Zhang *et al* 2005, 2006b, Duan *et al* 2007).

(2) In comparison with the predicted values of (Ω_n, μ_n) based on local model (solid line), positive and negative nonlocal models have opposite effects on the predicted values of (Ω_n, μ_n), and thus on the possibly excited flexural modes. The positive nonlocal model makes the (Ω_n, μ_n) curve of the CFMs steeper (dashed line) and accordingly higher modes are more likely excited while the negative nonlocal model makes the (Ω_n, μ_n) curve of the CFMs flatter (dotted line), and as a result lower modes are more likely excited.

(3) In either positive or negative nonlocal models, the larger the nonlocal length, the stronger the nonlocal effects on predicted (Ω_n, μ_n) values and mode transformation.

In the second step, a rigorous analysis of the nonlocal length effect on mode transformation is carried out in a quantitative sense. The critical curve $\mu = \mu(\Omega)$ to distinguish stable and unstable boundaries in the first and second regions of the Mathieu stability diagram is

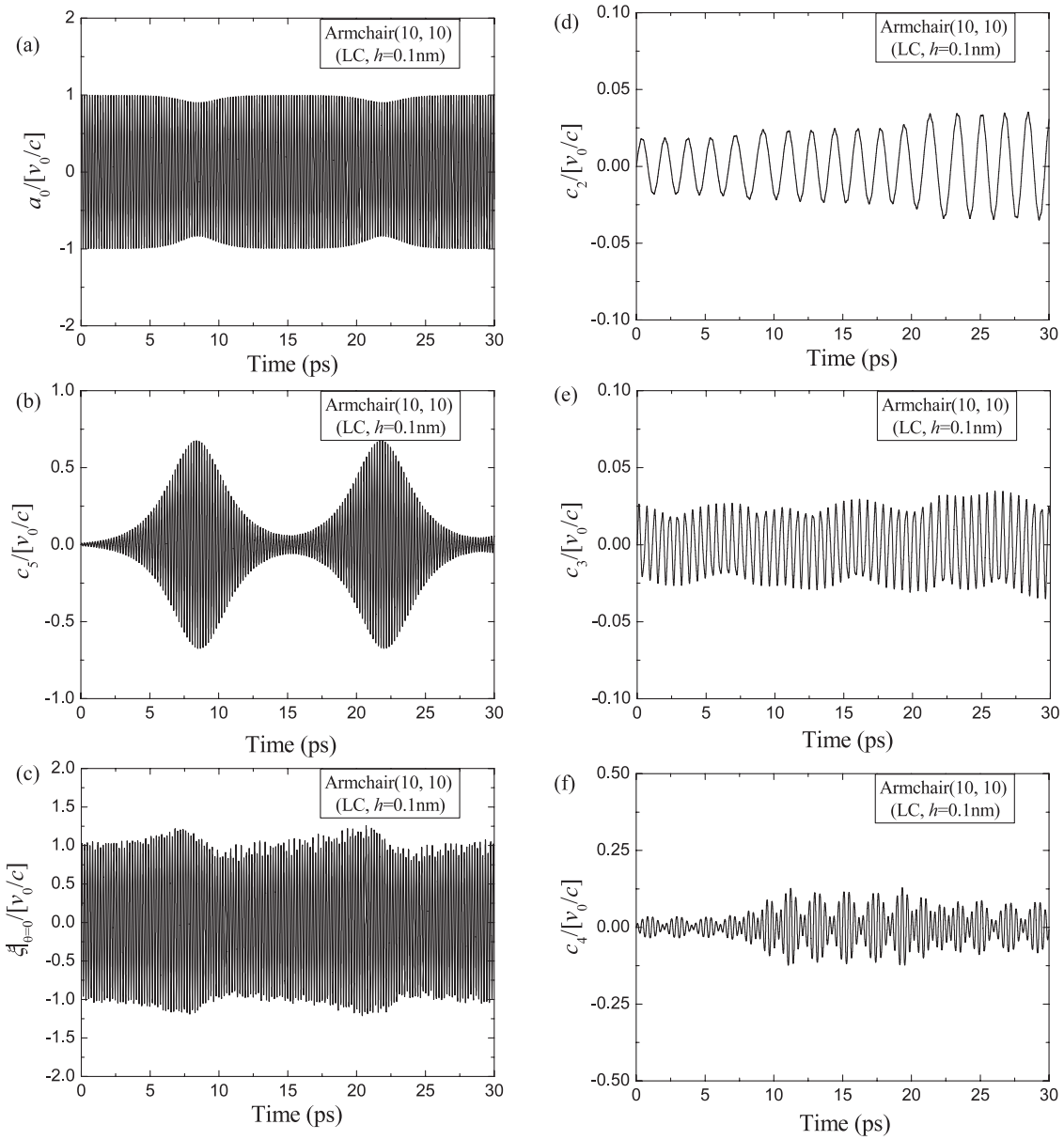

Figure 12. Response of armchair (10, 10) ($h = 0.1$ nm) within local model in real-time domain. (a) RBM, (b) CFM-5 and (c) total response at point $\theta = 0$ on middle surface ($v_0/c = 0.02$), (d) CFM-2, (e) CFM-3 and (f) CFM-4.

determined numerically by Floquet theory and asymptotic theory (McLachlan 1947, Struble 1962), as shown in figure 5. The analytical expression of $\mu = \mu(\Omega)$ based on asymptotic theory is given in McLachlan (1947), Struble (1962), i.e.

$$|1 - 2\omega| = \frac{\mu}{2\omega} \qquad \text{for region I} \tag{42}$$

and

$$\left|\frac{\mu^2}{2\omega(4\omega^2 - 1)} + 2(1 - \omega)\right| = \frac{\mu^2}{4\omega(2\omega - 1)} \qquad \text{for region II} \tag{43}$$

where $\omega = \sqrt{\Omega}$. We can then determine the critical initial velocity for a selection of armchairs from (8, 8) to (11, 11) based on three models, i.e. local elastic shell model, positive and negative nonlocal elastic shell models.

For a given armchair SWCNT and a given mode of CFM, the Ω_n value can be determined while the μ_n value depends on the initial velocity. In the Mathieu stability diagram defined by the critical curve $\mu = \mu(\Omega)$, CFM(s) with the lowest initial velocity beyond the critical curve is the most likely excited mode(s) in an elastic circular cylindrical shell. This method will be used to calculate the most likely excited CFM(s) for each of the selected armchairs. Two thickness values, 0.066 nm and 0.1 nm, are used, respectively, in the investigation exploring the possible influence of shell thickness in the nonlocal model on mode transformation. The representative nonlocal length of 0.1 nm determined previously (by fitting RBM frequency against MD simulations) is used. The most

Table 5. Most likely excited CFM(s) and the corresponding critical initial velocities for selected armchairs from (8, 8) to (10, 10) based on asymptotic critical curve of the Mathieu stability diagram. (Notes: (1) LC, NL(+) and NL(−) represent the results within local, positive or negative nonlocal models (use $l = 0.1$ nm), respectively; (2) I and II correspond to thicknesses $h = 0.066$ nm and 0.1 nm, respectively; (3) mode superscripted by $*$ indicates that it is excited in the second unstable region.)

	Mode (n)			Critical initial velocity (v_0/c)		
Armchair	LC	NL (+)	NL (−)	LC	NL(+)	NL(−)
(8, 8)						
I	4	5	4	0.0016	0.0081	0.0301
II	3	5	3	0.0250	0.0062	0.0119
(9, 9)						
I	4	5	4	0.0064	0.0044	0.0083
II	3	6	3	0.0323	0.0018	0.0272
(10, 10)						
I	4	6	4	0.0114	0.0009	0.0035
II	5^*	4	3	0.0059	0.0007	0.0349
(11, 11)						
I	5	7	4	0.0109	0.0012	0.0103
II	4	4	4	0.0106	0.0031	0.0285

likely excited CFM(s) above the critical curve for each of the selected armchairs is shown in table 5. In addition to the three observations based on figure 4, further observations are obtained based on the results given in table 5, i.e.

(4) Mode transformation is very sensitive to the thickness and radius of the shell. Normally, with the decrease of the aspect ratio α (i.e. the shell becomes thinner), the higher mode(s) of CFM(s) is more likely excited. However, exceptions exist in local and positive nonlocal models. For example, the most likely excited mode in armchair (10, 10) changes from 5 to 4 when the thickness decreases from 0.1 to 0.066 nm according to the local model. In another example, the most likely excited mode in armchair (9, 9) changes from 6 to 5 when the thickness decreases from 0.1 to 0.066 nm according to the positive nonlocal model.

(5) The positive nonlocal model does not surely predict the excitation of a higher flexural mode than the local model. For instance, in armchair (10, 10) with thickness 0.1 nm, flexural mode 4 is likely excited according to the positive nonlocal model in contrast to mode 5 predicted by the local model. However, it seems that the negative nonlocal model consistently predicts a lower or equal flexural mode to be excited when compared to the local model.

The most likely excited CFMs are shown in table 5 for armchairs from (8, 8) to (10, 10). The data in table 5 show that, for armchair (10, 10), the local model predicts the excitation of CFM 5 in the second unstable region of the Mathieu stability diagram. However, both nonlocal models predict the excitation of CFMs in the first unstable region. This explains why observation (5) seems to contradict observation (2).

Clearly it can be seen from the calculated results in table 5 that, given a circular cylindrical shell (with fixed thickness and radius), different CFMs may be excited according to different continuum models, and therefore it is necessary to employ a more reliable tool to evaluate which one among the three models is most appropriate for SWCNTs. MD simulations using commercial software *Material Studio* (Accelrys 2008) with the module *Forcite Plus* and the atomistic force field *COMPASS*. Sun (1998), Sun *et al* (1998) is again employed for this purpose. The same group of armchairs from (8, 8) to (11, 11) are investigated and each of them is assumed to be infinitely long so that a lattice unit structure is used in the study. When the initial pure RBM vibration is introduced, the subsequent vibration process is observed through the module (Shi *et al* 2009). An initial RBM velocity as low as possible is imposed such that the most likely excited CFM can be captured if it is excited. The time step taken is 1 fs and the simulation time runs up to 100 ps. The configuration of each lattice unit when CFM is excited and the excitation time are shown in figure 6.

It is found that CFM-3 is excited for all examined armchairs from (8, 8) to (11, 11). According to the results in table 5, only the negative nonlocal model (with nonlocal length 0.1 nm) is able to predict the excitation of CFM-3 for armchairs (8, 8) to (10, 10), though the predicted mode for armchair (11, 11) based on the negative nonlocal model is CFM-4, which is different from the MD prediction of CFM-3. The positive nonlocal model does not predict CFM-3 for all the armchairs examined. Since a nonlocal length of 0.1 nm is used, predictions in table 5 are related only to this nonlocal length value. Therefore a detailed analysis of mode transformation with various nonlocal lengths is necessary. A range of 0–0.5 nm of nonlocal length with a resolution 0.001 nm is used to identify the most likely excited CFMs for the same group of armchairs. Two thickness values, 0.066 nm and 0.1 nm, are used again for all armchairs, respectively. For each nonlocal length within the range of 0–0.5 nm, the most likely excited CFM and the normalized critical initial velocity are plotted. Results for the sub-range (0, 0.2 nm) are presented in figures 7–10 for demonstration purposes. Graphs (a) in the above figures show the CFMs (CFM-3 to CFM-5 or CFM-6) to be excited based on the negative nonlocal model and the required critical initial velocity. Graphs (b) and (c) in all the figures correspond to predictions based on the positive nonlocal model for armchairs with thicknesses 0.066 nm and 0.1 nm, respectively. For all the cases within the positive nonlocal model, higher modes (higher than 6) are found to be occasionally excited and the critical initial velocity varies continuously for lower modes when nonlocal length is small. However, as nonlocal length increases, the excited flexural modes decrease (e.g. in the case of armchair (10, 10) with thickness either 0.066 or 0.1 nm, the excited mode changes from 5 to 4 around a nonlocal length 0.14 nm and then from 4 to 3 around a nonlocal length 0.18). At these special nonlocal lengths, where excited mode number decreases, critical initial RBM vibration velocity increases sharply. This discontinuous characteristic of critical initial velocity in the positive nonlocal model is evidently in contrast to the continuity of the critical initial velocity in the negative nonlocal model, which can be explained by observation (2), or by figure 4, i.e. the larger the nonlocal length, the steeper the critical initial velocity curve within the positive nonlocal model but the flatter within the negative nonlocal model.

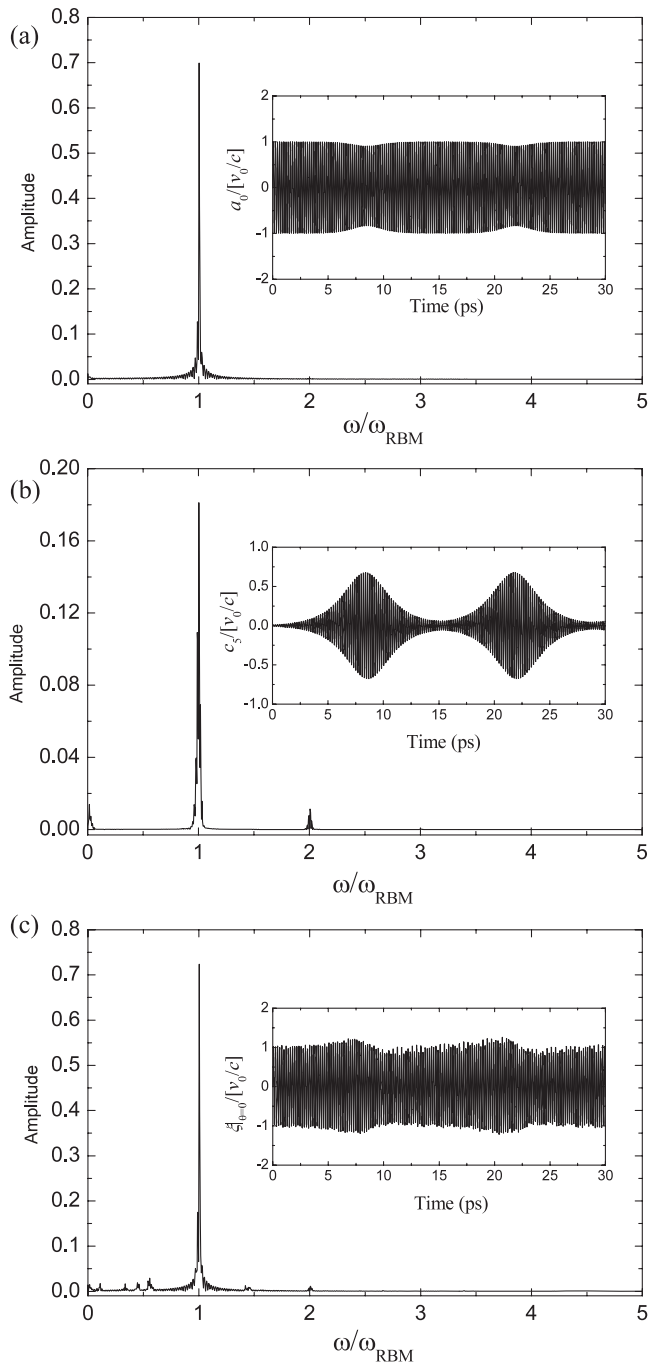

Figure 13. Response of armchair (10, 10) ($h = 0.1$ nm) within the local model in frequency domain. (a) RBM, (b) CFM-5 and (c) total response at point $\theta = 0$ on the middle surface. ($v_0/c = 0.02$.)

It may be necessary to point out that, since CFMs are mainly excited in the first two unstable regions (especially the first one) of the Mathieu stability diagram and the estimated critical initial velocity is quite small (normally of the order of 0.01), the above procedure using asymptotic critical velocity curves to determine the excited CFMs is reliable. However, the calculated critical initial velocity may not be so accurate since the discarded nonlinear couplings may become remarkably pronounced when they are accounted for, which will be shown in section 6.

Detailed analyses of the nonlocal length effect on mode transformation of the selected armchairs, as shown in figures 7–10, reveal that, as nonlocal length increases, CFMs from 3 to 6 and occasionally higher modes can be excited in individual armchairs. Since MD simulations show that only CFM-3 is excited for all the selected armchairs, we need to find a common sub-range of nonlocal lengths in which the right nonlocal model can predict similar results for all the armchairs with thickness either 0.066 or 0.1 nm. The sub-range of 0–0.5 nm for each of the four cases (i.e. individual armchairs with thickness either 0.066 or 0.1 nm, based on either positive or negative nonlocal models) is searched and the results are shown in table 6, in which CFM-3 will be excited in all the armchairs. For the situation when two or more sub-ranges are found, if the gap between the successive sub-ranges is rather narrow, the possibility that other modes are excited in this small gap is rare. Therefore, the separated sub-ranges will be united by neglecting the small gaps. For instance, in the case of armchair (8, 8) with thickness 0.066 nm based on the negative nonlocal model, originally two sub-ranges 0.114–0.195 nm and 0.199–0.261 nm are found for CFM-3. Since the gap 0.196–0.198 is very narrow, it is neglected and then one united sub-range 0.114–0.261 nm is taken. The final four common sub-ranges are found for the four cases and are also given in table 6. Three common sub-ranges (for the cases based on both nonlocal models when the thickness is 0.066 nm and based on the positive nonlocal model when the thickness is 0.1 nm) are very narrow and hence are discarded. The valid one is 0.122–0.259 nm for the case of armchairs with thickness 0.1 nm based on the negative nonlocal model. Actually, for the valid case, the first three armchairs give a common sub-range 0.071–0.259 nm and the armchair (11, 11) upgrades the lower limit to 0.122 nm. It is shown again that the negative second-order nonlocal model should be adopted for the nonlocal modelling of SWCNTs. Furthermore, thickness 0.1 nm, rather than 0.066 nm, is appropriate to SWCNTs as far as mode transformation is concerned.

5. Discussion of nonlocal length

Before numerical examples of the mode transformation are shown in section 6, further discussion on nonlocal length is necessary. It has been shown that different nonlocal lengths have been determined for RBM and CFMs from the frequency analysis while a range of nonlocal lengths is obtained based on mode transformation analysis. According to classical nonlocal elasticity theories (Eringen 1983b) and their applications to CNTs (Zhang *et al* 2004, Wang and Hu 2005, Zhang *et al* 2005), nonlocal length as an intrinsic length of material microstructure should be unique to SWCNTs. However, the present study and other publications in the literature (Duan *et al* 2007, Hu *et al* 2008) clearly show that nonlocal length is dependent on vibration mode number. When mode transformations appear during the vibration of an SWCNT, RBM and one or more CFMs will be involved in the vibration process. It seems inconsistent in mode transformation analysis when a fixed nonlocal length is adopted. However, if one discards the fixed nonlocal length assumption and takes it as a

Table 6. Nonlocal length intervals within which CFM-3 is predicted to be excited by the positive and negative nonlocal models. Two thickness values, 0.066 and 0.1 nm, are considered for all armchairs from (8, 8) to (11, 11). NL(−) and NL(+) correspond to negative and positive nonlocal models, respectively.

	$h = 0.066$ nm		$h = 0.1$ nm	
Armchair	NL(−)	NL(+)	NL(−)	NL(+)
(8, 8)	0.114–0.261	0.145–0.205	0.001–0.259	0.001–0.056 0.145–0.205
(9, 9)	0.160–0.294	0.164–0.230	0.001–0.292	0.001–0.026 0.164–0.230
(10, 10)	0.207–0.326	0.182–0.256	0.071–0.325	0.182–0.256
(11, 11)	0.256–0.347	0.200–0.281	0.122–0.358	0.200–0.281
Common sub-range	0.256–0.261	0.200–0.205	0.122–0.259	0.200–0.205

function of vibration modes, it makes the problem dramatically complicated, which is outside the scope of the present research.

In order to overcome the limitation of the negative nonlocal model with fixed nonlocal length, we performed a probability analysis of the most likely excited CFMs in armchair SWCNTs from (8, 8) to (11, 11) with thickness 0.1 nm based on the Mathieu stability diagram. The analysis results are presented in figure 11. It is shown that, as nonlocal length varies from 0 to 0.5 nm in a step of 0.001 nm, only CFM-3, CFM-4 and CFM-5 are excited and their excitation probabilities are 83.2%, 11.1% and 5.7%, respectively. Therefore, regardless of the specific value of nonlocal length in 0–0.5 nm, the excitation probability of CFM-3 is dominant based on the negative nonlocal model, which agrees well with MD predictions.

6. Numerical examples of mode transformation

Now we have found that the negative second-order strain gradient nonlocal model is appropriate for armchairs with thickness 0.1 nm. Nonlocal length in the model can be given as 0.1 nm in an average sense since RBM is the principal vibration mode (it is also within the required common range for armchairs (8, 8) to (10, 10)). Next, armchair (10, 10) is taken as the example to show the mode transformation phenomenon based on local and negative nonlocal models, respectively. The fourth-order Runge–Kutta method is employed to solve the original governing differential equations (17)–(19) under initial conditions given in equation (37). In order to compare numerical solutions from the two models, the imperfections in equation (37) are fixed at exactly two orders smaller than the initial RBM velocity. The same stochastically produced imperfections are prescribed in the two models.

The initial RBM velocity v_0/c is given as 0.02 and 0.04, respectively, in the calculations based on local and negative nonlocal models. The required initial velocities in the two models are predicted as 0.0059 and 0.0349 (see table 5), respectively. The given initial RBM velocity for the local model is much higher than the required one. This is simply because a fast mode transformation is sought in the calculation. It is actually found that, when the initial RBM velocity in the local model is given just slightly larger than the required value (use 0.006 in the real calculation), mode transformations emerge nearly 10 times slower and the amplitude of the excited CFM-5 is very small. Therefore, a larger value is preferred on the premise that a convergent solution can be obtained and 0.02 is selected after a few trials.

Graphs (a)–(c) in figures 12 and 14, respectively, are the time domain responses of RBM and the excited dominant CFM at point $\theta = 0$ on the middle surface. Responses of nearby CFMs around the dominant one are also plotted in the remaining three graphs (d)–(f) in these two figures in order to compare the amplitudes between the dominant CFM, which is supposed to be the most likely excited CFM based on the Mathieu stability diagram, and other nearby CFMs, which should be much smaller in amplitude. Just as predicted by the Mathieu stability diagram, modes 5 and 3 are the most likely excited CFMs in armchair (10, 10) with thickness 0.1 nm from local and nonlocal models, respectively. Other nearby CFMs have much smaller amplitudes than the dominant one. The coupled vibrations of RBM and CFMs at a point on the middle surface are shown in graph (c) of the two figures.

Frequency domain responses of RBM and the dominant flexural mode at the same point on the middle surface are shown in figures 13 and 15, respectively. It can be seen from figure 13 that, for the case of armchair (10, 10) with thickness 0.1 nm in the local model, only one major peak appears at roughly the same point in all three vibration frequency spectra. It implies that the excited dominant CFM-5 has approximately the same frequency as the prime vibration mode, RBM. This can be easily understood by means of the Mathieu stability diagram. As discussed in section 4, CFM-5 is the most likely excited mode in armchair (10, 10) with thickness 0.1 nm in the local model, which occurs in the *second* unstable region of the Mathieu stability diagram, i.e. $\Omega_n \approx 1$ ($n = 5$). Ω_n is the dominant term in the coefficient of c_n (i.e. $\Omega_n - \mu_n \sin \eta$) in equation (39). It can be deduced that the circular frequency of the vibration of c_n is approximately the RBM frequency. However, for the same armchair in the negative nonlocal model, as shown in figure 15, the excited CFM-3 has a frequency approximately half of the RBM frequency. Accordingly, there are two evident frequency peaks in the vibration spectrum of the point $\theta = 0$ on the middle surface. This phenomenon can also be explained with the help of the Mathieu stability diagram. In this case, the most likely excited CFM will happen in the first unstable region around $\Omega_n \approx 0.25$. Accordingly, the solution of c_n in equation (39) will possess a normalized circular frequency of around 0.5, i.e. a circular frequency of around half of the RBM frequency.

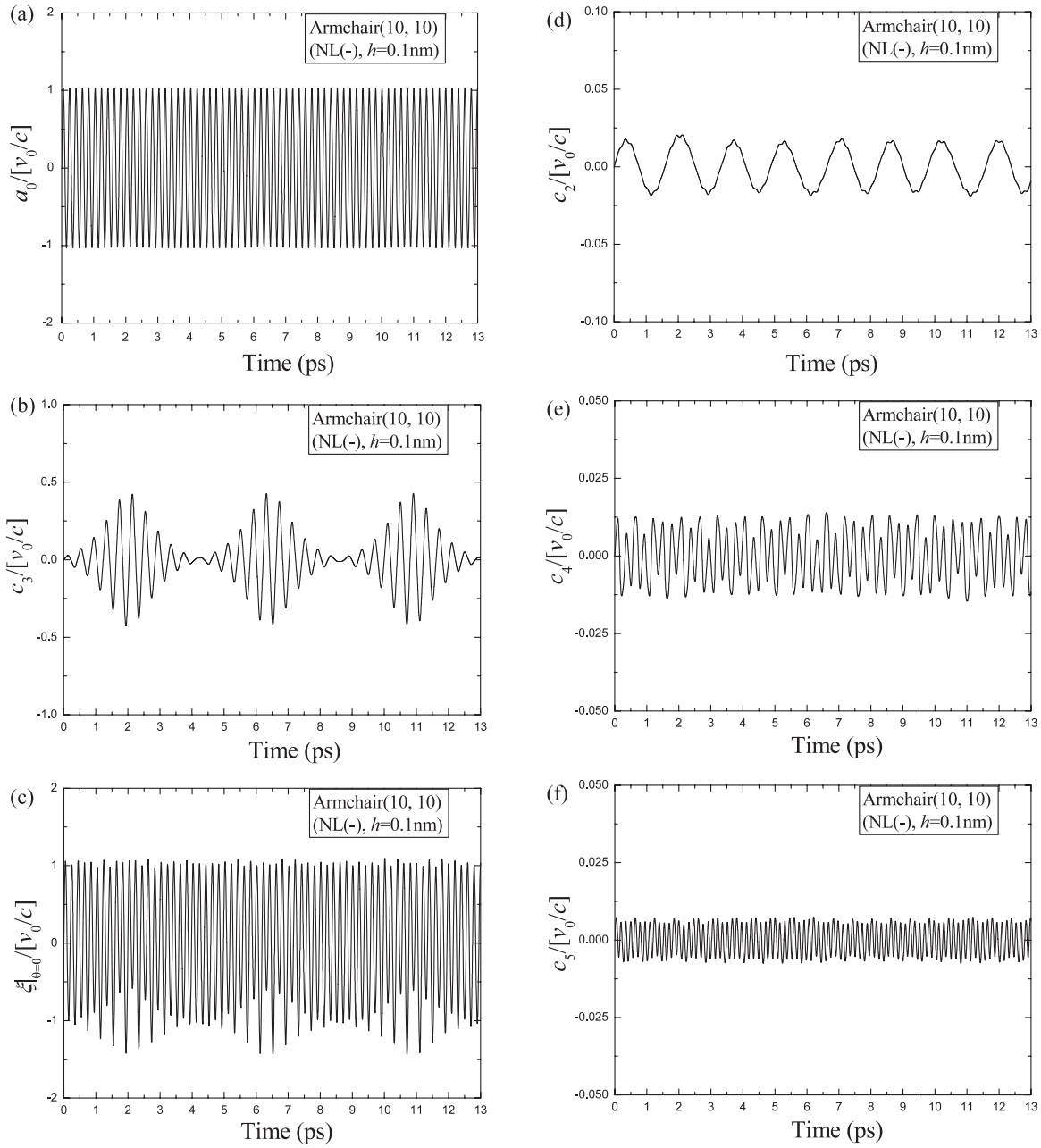

Figure 14. Response of armchair (10, 10) ($h = 0.1$ nm) within the negative nonlocal model in real-time domain ($l = 0.1$ nm). (a) RBM, (b) CFM-3 and (c) total response at point $\theta = 0$ on the middle surface. ($v_0/c = 0.04$.) (d) CFM-2, (e) CFM-4 and (f) CFM-5.

These numerical examples show that mode interaction and mode transformation exist in nanoscale structures like SWCNTs. When the RBM vibration amplitude is sufficiently high, it may become unstable and then nearby CFMs are excited. Similar to macroscopic thin circular cylindrical shells (Nayfeh and Raouf 1987, Amabili *et al* 2000), 1:1 and 2:1 internal resonance phenomena may occur in SWCNTs simulated respectively by local and nonlocal models. Therefore, the internal resonance mechanism is model-dependent. By referring to the MD simulations, the negative nonlocal model is found to be appropriate to SWCNTs. As a result, armchair (10, 10) with thickness 0.1 nm is shown to possess a 2:1 internal resonance mechanism.

7. Conclusions

Based on the second-order strain gradient nonlocal constitutive equation between stress and strain, a nonlocal circular cylindrical shell model is established by extending the original Goodier and McIvor's thin circular cylindrical shell theory to a nonlocal version. Between the positive and negative second-order strain gradient nonlocal models, it is found that the negative nonlocal model is appropriate to armchair SWCNTs with thickness 0.1 nm. Furthermore, the nonlocal length is determined by fitting RBM frequency against MD simulations and a representative nonlocal length approximately 0.1 nm in an average sense is obtained. When frequencies of

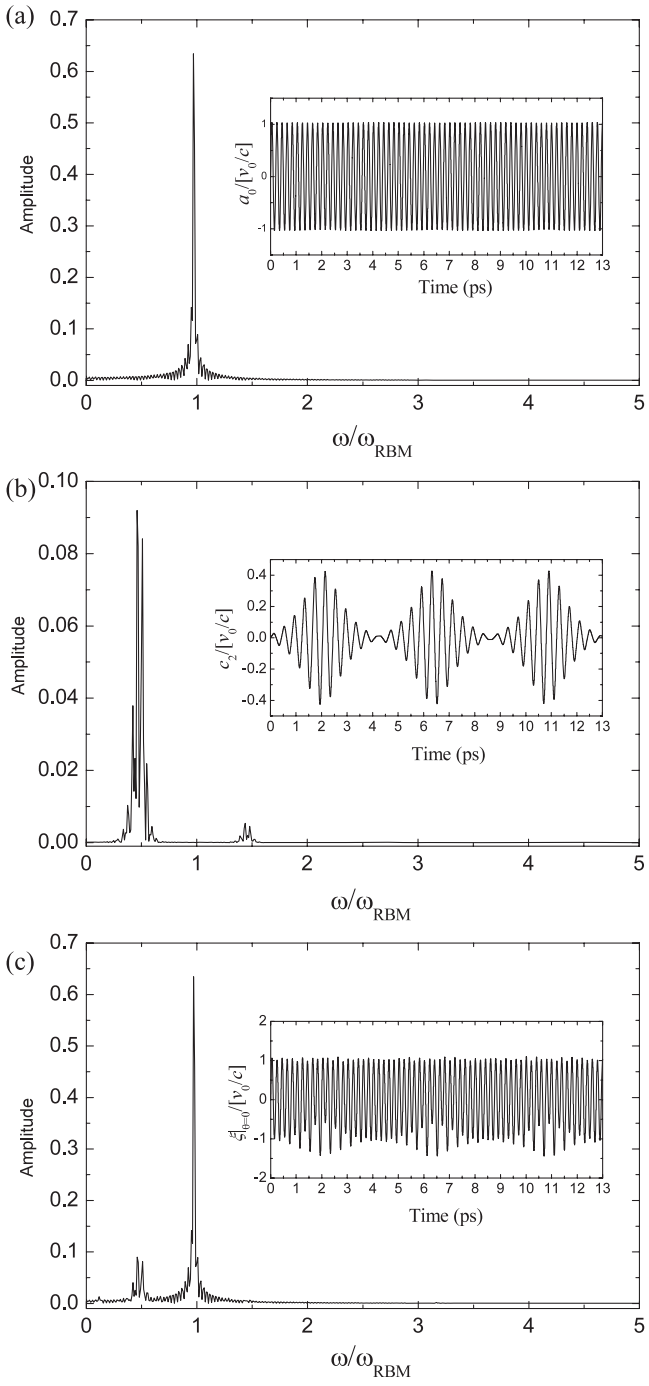

Figure 15. Response of armchair (10, 10) ($h = 0.1$ nm) within the negative nonlocal model in frequency domain ($l = 0.1$ nm). (a) RBM, (b) CFM-3 and (c) total response at point $\theta = 0$ on the middle surface. ($v_0/c = 0.04$.)

CFMs are evaluated, nonlocal length is found to be dependent on the flexural modes for a given SWCNT. Both frequency analyses show that the nonlocal length is also related to the radius-to-thickness ratio. When the nonlocal effect on mode transformation is investigated, a range of 0.122–0.259 nm is obtained for the nonlocal length in the negative second-order nonlocal model. The representative nonlocal length 0.1 nm based on RBM frequency analysis can predict the same mode transformation as in MD simulations. Finally, 1:1 and 2:1 internal resonance mechanisms through numerical examples are demonstrated for local and negative nonlocal models, respectively, which indicates that the internal resonance mechanism depends on the continuum models employed.

Acknowledgment

MXS acknowledges the financial support from Dorothy Hodgkin Postgraduate Award (EPSRC-Shell DHPA).

References

Accelrys 2008 http://Accelrys.Com/Products/Materials-Studio/ Accessed on 30 April 2009

Amabili M, Pellicano F and Vakakis A F 2000 Nonlinear vibrations and multiple resonances of fluid-filled, circular shells, part 1: equations of motion and numerical results *Trans. ASME, J. Vib. Acoust.* **122** 346–54

Askes H and Aifantis E C 2006 Gradient elasticity theories in statics and dynamics a unification of approaches *Int. J. Fract.* **139** 297–304

Askes H, Suiker A S J and Sluys L J 2002 A classification of higher-order strain-gradient models—linear analysis *Arch. Appl. Mech.* **72** 171–88

Brenner D W, Shenderova O A, Harrison J A, Stuart S J, Ni B and Sinnott S B 2002 A second-generation reactive empirical bond order (Rebo) potential energy expression for hydrocarbons *J. Phys.: Condens. Matter* **14** 783–802

Duan W H, Wang C M and Zhang Y Y 2007 Calibration of nonlocal scaling effect parameter for free vibration of carbon nanotubes by molecular dynamics *J. Appl. Phys.* **101** 024305

Eringen A C 1983a On differential-equations of nonlocal elasticity and solutions of screw dislocation and surface-waves *J. Appl. Phys.* **54** 4703–10

Eringen A C 1983b Theories of nonlocal plasticity *Int. J. Eng. Sci.* **21** 741–51

Goodier J N and McIvor I K 1964 The elastic cylindrical shell under nearly uniform radial impulse *J. Appl. Mech.* **31** 259–66

Hu Y G, Liew K M, Wang Q, He X Q and Yakobson B I 2008 Nonlocal shell model for elastic wave propagation in single- and double-walled carbon nanotubes *J. Mech. Phys. Solids* **56** 3475–85

Ioannidou T, Pouget J and Aifantis E 2001 Kink dynamics in a lattice model with long-range interactions *J. Phys. A: Math. Gen.* **34** 4269–80

Kurti J 1998 First-principles calculations of the radial breathing mode of single-wall carbon nanotubes *Phys. Rev.* B **58** R8870

Kuzmany H, Burger B, Thess A and Shalley R E 1998 Vibrational spectra of single wall carbon nanotubes *Carbon* **36** 709–12

Lawler H M, Areshkin D, Mintmire J W and White C T 2005 Radial-breathing mode frequencies for single-walled carbon nanotubes of arbitrary chirality: first-principles calculations *Phys. Rev.* B **72** 233403

Li Q M and Shi M X 2008 Intermittent transformation between radial breathing and flexural vibration modes in a single-walled carbon nanotube *Proc. R. Soc.* A **464** 1941–53

McIvor I K 1966 Elastic cylindrical shell under radial impulse *J. Appl. Mech.* **33** 831–7

McLachlan N W 1947 *Theory and Application of Mathieu Functions* (Oxford: Clarendon)

Metrikine A V and Askes H 2002 One-dimensional dynamically consistent gradient elasticity models derived from a discrete microstructure part 1: generic formulation *Eur. J. Mech.* A **21** 555–72

Nayfeh A H and Raouf R A 1987 Non-linear oscillation of circular cylindrical-shells *Int. J. Solids Struct.* **23** 1625–38

Rao A M, Richter E, Bandow S, Chase B, Eklund P C, Williams K A, Fang S, Subbaswamy K R, Menon M, Thess A, Smalley R E, Dresselhaus G and Dresselhaus M S 1997 Diameter-selective Raman scattering from vibrational modes in carbon nanotubes *Science* **275** 187–91

Sanchez-Portal D, Artacho E, Soler J M, Rubio A and Ordejon P 1999 *Ab initio* structural, elastic, and vibrational properties of carbon nanotubes *Phys. Rev.* B **59** 12678–88

Shi M X, Li Q M and Huang Y 2009 Internal resonance of single-walled carbon nanotubes *Proc. R. Soc.* A **465** 3069–82

Struble R A 1962 *Nonlinear Differential Equations* (New York: McGraw-Hill)

Sudak L J 2003 Column buckling of multiwalled carbon nanotubes using nonlocal continuum mechanics *J. Appl. Phys.* **94** 7281–7

Sun H 1998 Compass: an *ab initio* force-field optimized for condensed-phase applications—overview with details on alkane and benzene compounds *J. Phys. Chem.* B **102** 7338–64

Sun H, Ren P and Fried J R 1998 The Compass force field: parameterization and validation for phosphazenes *Comput. Theor. Polym. Sci.* **8** 229–46

Tounsi A, Heireche H, Berrabah H M, Benzair A and Boumia L 2008 Effect of small size on wave propagation in double-walled carbon nanotubes under temperature field *J. Appl. Phys.* **104** 104301

Wang C M, Zhang Y Y and He X Q 2007 Vibration of nonlocal Timoshenko beams *Nanotechnology* **18** 105401

Wang C Y, Ru C Q and Mioduchowski A 2005 Axisymmetric and beamlike vibrations of multiwall carbon nanotubes *Phys. Rev.* B **72** 075414

Wang C Y and Zhang L C 2008 A critical assessment of the elastic properties and effective wall thickness of single-walled carbon nanotubes *Nanotechnology* **19** 075705

Wang L F and Hu H Y 2005 Flexural wave propagation in single-walled carbon nanotubes *Phys. Rev.* B **71** 195412

Wang Q 2005 Wave propagation in carbon nanotubes via nonlocal continuum mechanics *J. Appl. Phys.* **98** 124301

Wang Q, Zhou G Y and Lin K C 2006 Scale effect on wave propagation of double-walled carbon nanotubes *Int. J. Solids Struct.* **43** 6071–84

Xie G Q, Han X and Long S Y 2007 Effect of small size on dispersion characteristics of wave in carbon nanotubes *Int. J. Solids Struct.* **44** 1242–55

Yakobson B I, Brabec C J and Bernholc J 1996 Nanomechanics of carbon tubes: instabilities beyond linear response *Phys. Rev. Lett.* **76** 2511–4

Zhang X, Jiao K, Sharma P and Yakobson B I 2006a An atomistic and non-classical continuum field theoretic perspective of elastic interactions between defects (force dipoles) of various symmetries and application to graphene *J. Mech. Phys. Solids* **54** 2304–29

Zhang Y Q, Liu G R and Han X 2006b Effect of small length scale on elastic buckling of multi-walled carbon nanotubes under radial pressure *Phys. Lett.* A **349** 370–6

Zhang Y Q, Liu G R and Wang J S 2004 Small-scale effects on buckling of multiwalled carbon nanotubes under axial compression *Phys. Rev.* B **70** 205430

Zhang Y Q, Liu G R and Xie X Y 2005 Free transverse vibrations of double-walled carbon nanotubes using a theory of nonlocal elasticity *Phys. Rev.* B **71** 195404